Supplementary Information (SI) for Journal of Materials Chemistry A.
This journal is © The Royal Society of Chemistry 2025

Supporting Information

Establishing Long-Term Stable Cathode-Electrolyte Interphase through Multi-Cationic Competitive Coordination for 4.6 V $LiCoO_2$

Yujie Wang[a], Tingting Cui*[a], Netanel Shpigel[c], Zihao Meng[a], Fuhui Liang[a], Tianju Fan*[a, b] and Yonggang Min*[a, d]

a. School of Materials and Energy, Guangdong University of Technology, Guangzhou, 510006, PR China.
E-mail: 2112202211@mail2.gdut.edu.cn (Y. Wang), cuitt@gdut.edu.cn (T. Cui), ygmin@gdut.edu.cn (Y. Min), tianjufan@gmail.com (T. Fan)

b. Automotive Engineering Research Institute, BYD Automobile Industry Co., Ltd. Shenzhen 518000, P. R. China.
E-mail: tianjufan@gmail.com (T. Fan)

c. Ariel University, Ariel 40700, Israel.
E-mail: nshpigel@gmail.com (N.Shpigel)

d. Guangzhou Liangyue Materials Technology Co., Ltd. Guangzhou 510663, China.
E-mail: ygmin@gdut.edu.cn (Y. Min)

Experimental

Preparation of Electrolytes and LCO Cathode Electrodes

The conventional carbonate-based electrolyte (1 M LiPF6, FEC/ DMC, v: v= 1: 4) was used as a baseline. RbF purchased from J&K, was added into the baseline electrolyte with different mass fractions (1%, 2%, 5%). The LCO cathodes were fabricated by mixing $LiCoO_2$ powder, Super P (conductive agent), and polyvinylidene fluoride (PVDF, binder) with a weight ratio of 80: 10: 10 with N-methyl-2-pyrrolidone (NMP) as solvent. The slurry then was coated in a current collector (aluminum foil) and dried at 120°C overnight in a vacuum oven. The obtained electrodes were punched into disks with a diameter of 12 mm and then rolled, with a typical mass loading of 3.0- 5.0 mg cm^{-2}. To eliminate the trace amounts of water, the LCO cathodes were further baked in a vacuum oven at 110 °C for 2 h before use.

Electrochemical Measurements

The electrochemical performance was assessed in a coin-type CR2032 cell and in an Ar-filled glovebox (O_2 and moisture content below 0.1 ppm) with the Celgard 2500 separator and 120 μL electrolyte for each cell. CR2032 coin cells with Li metal as an anode were used to evaluate the electrochemical performance. Li‖LCO batteries with Li metal as an anode were used to evaluate the electrochemical performance. The batteries were evaluated by a NEWARE cell testing instrument (BTS- 5 V 10 mA). The cells were tested by a galvanostatic method with 0.5 C charging and discharging (0.1 C charging–discharging for the initial 3 cycles) between 3 and 4.6 V at room temperature. Linear sweep voltammogram (LSV) and Cyclic voltammograms (CV) were performed on the

CHI760E electrochemical workstation to analyse the redox characteristics of electrolytes. The CV curves were collected at 4 mV s^{-1} from 3- 4.6 V and the LSV curves were collected at 1 mV s^{-1} from 3- 5.5 V. Electrochemical impedance spectroscopy (EIS) tests were performed on the CHI760E electrochemical workstation. The EIS tests were performed on as-assembled cells and cells that had been activated for 200 cycles. The AC amplitude in EIS tests was set at 5 mV within a frequency range of 100 kHz to 0.01 Hz.

Materials Characterization

The cycled Li||LCO cells with different electrolytes were disassembled in a glovebox filled with Ar, followed by washing with dimethyl carbonate (DMC, for LCO cathodes) three times to remove residual lithium salts. X-ray diffraction (XRD, Bruker D8 ADVANCE) was conducted on pristine and cycled LCO cathodes for phase identification and peak intensity ratios were calculated by the ratio of peak areas after background subtraction. A field emission scanning electron microscope (FESEM, Apreo 2S HiVac) was performed to examine the surface morphology. To access the detailed morphologies and identify the elemental compositions of cathode materials, High Resolution Transmission Electron Microscope (HRTEM, FEI Talos F200x) was conducted. An ex-situ X-ray photoelectron spectrometer (XPS, Thermo Fisher Escalab 250Xi) was used to analyze the surface chemistry of the cycled LCO electrodes.

Simulations

All density functional theory (DFT) calculations were performed using the Vienna Ab Initio Simulation Package (VASP)[1] with the HZW (DS-PAW)[2] method. The electronic exchange-correlation interactions were described using the spin-polarized generalized gradient approximation (GGA) with the Perdew-Burke-Ernzerhof (PBE) functional. To account for the localized d-electron states of transition metals, the GGA + U approach was employed, setting the U value for Co 3d states to 4.9 eV.[3, 4] A plane-wave energy cutoff of 500 eV was used, and Brillouin zone integrations were carried out using a Monkhorst-Pack k-point grid of 12*12*3. The LCO was modeled as a single unit cell with a space group of $R\bar{3}m$.Lattice parameters and atom position were fully relaxed until the force on each atom was less than 0.01 eV $Å^{-1}$.

In order to perform molecular dynamics simulations, an amorphous cell module was utilized to construct a solvation structure comprising 1,622 atoms with a density of 0.4 g cm^{-3}. The initial configuration underwent energy minimization using a conjugate gradient method, with a convergence criterion set to $1.0*10^{-4}$. The electrolyte used was a 1 M $LiPF_6$ solution in dimethyl carbonate (DMC) and fluoroethylene carbonate (FEC). Although the thermodynamic melting point of this mixed solution is approximately 298 K, the limits of the kinetic liquid range could be lower, thereby enabling liquid state simulations at room temperature.

Based on the Forcite module, simulations were conducted under the isothermal-isobaric (NPT) ensemble, maintaining a pressure of 1 bar and a temperature of 298 K using the Parrinello-Rahman barostat.[5] The equilibration time was set to 500 ps with a time constant of 1 fs. An annealing process was further employed to ensure the melting of all systems, avoiding local configurational constraints. All systems were heated from 298 K to 400 K and held for 500 ps. Finally, production runs were conducted under the Nose-Hoover thermostat (time constant of 1

ps), set at a temperature of 298 K for a duration of 5 ns to ensure sufficient sampling of all systems' diffusion states.

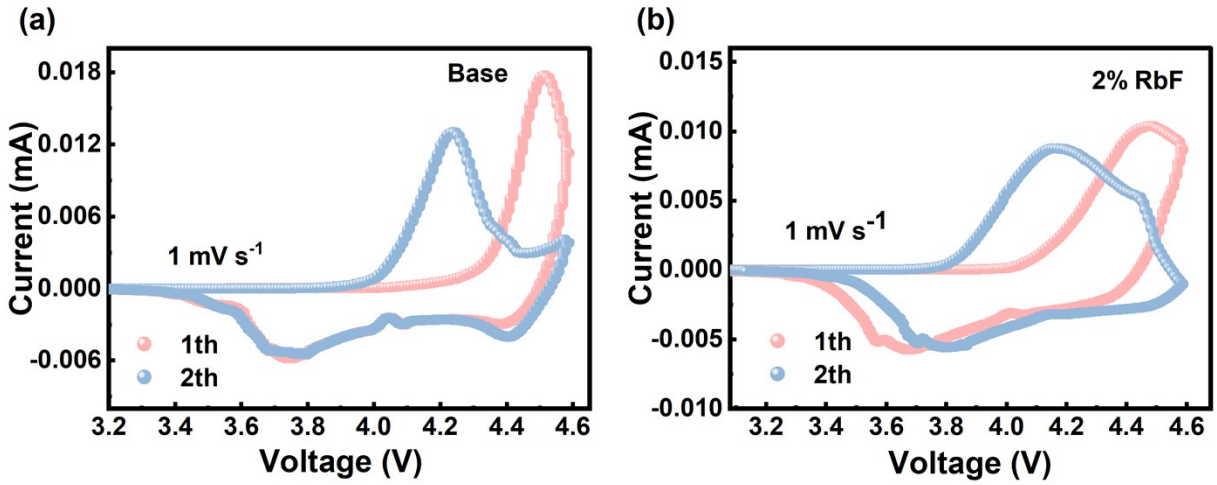

Figure S1. The cyclic voltammetry in (a) base electrolyte and (b) 2% RbF electrolyte.

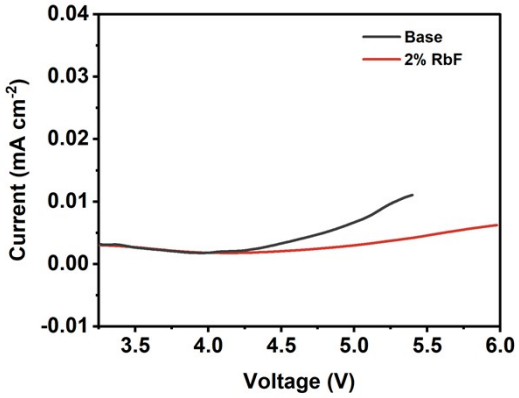

Figure S2. The linear sweep voltammetry (LSV) of base and 2% RbF electrolytes.

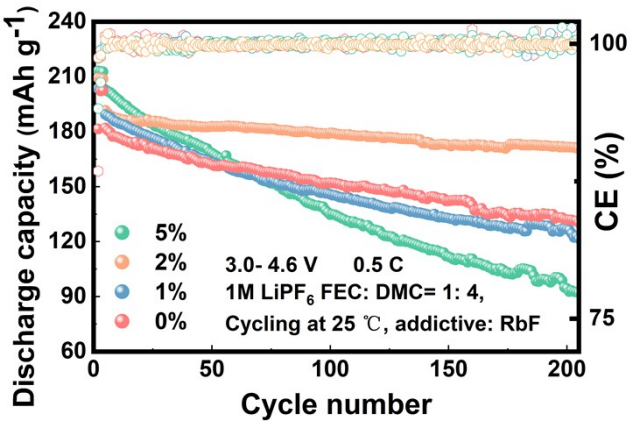

Figure S3. The cycling performances of Li||LCO batteries in 0~ 5 wt% RbF electrolytes at an operating voltage of 3 ~ 4.6 V and 0.5 C.

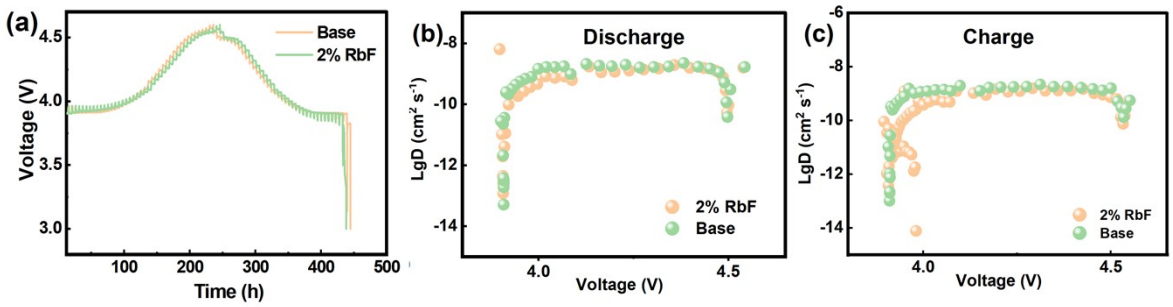

Figure S4. Galvanostatic intermittent titration technique (GITT) curves of $LiCoO_2$ in based and 2% RbF electrolyte using a pulse current of 0.05C for 30 min and internals of 5h in a stable cycle. The corresponding Li^+ diffusion coefficients (D_{Li+}) of LCO batteries at discharging (b) and charging (c) with these two electrolytes.

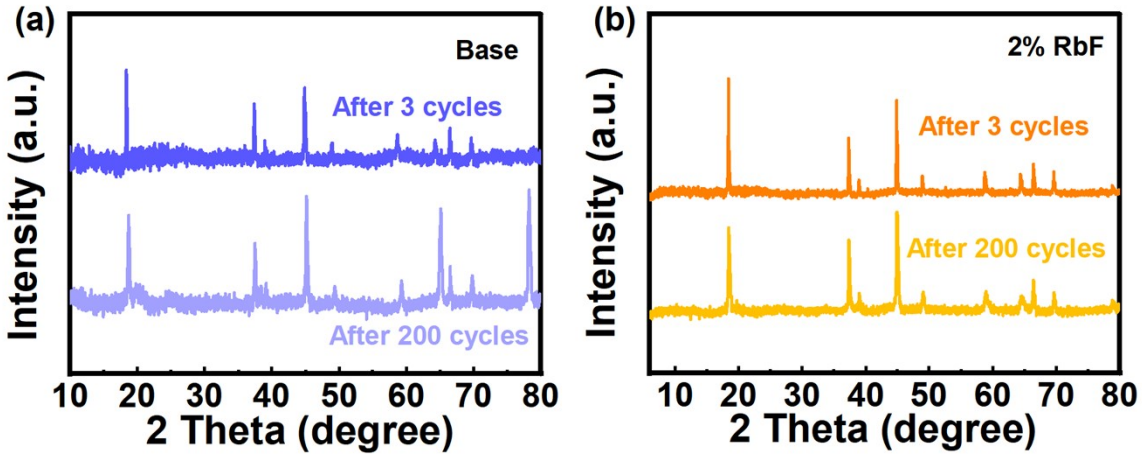

Figure S5. XRD of LCO cathodes after 3 and 200 cycles in baseline and 2%RbF electrolytes.

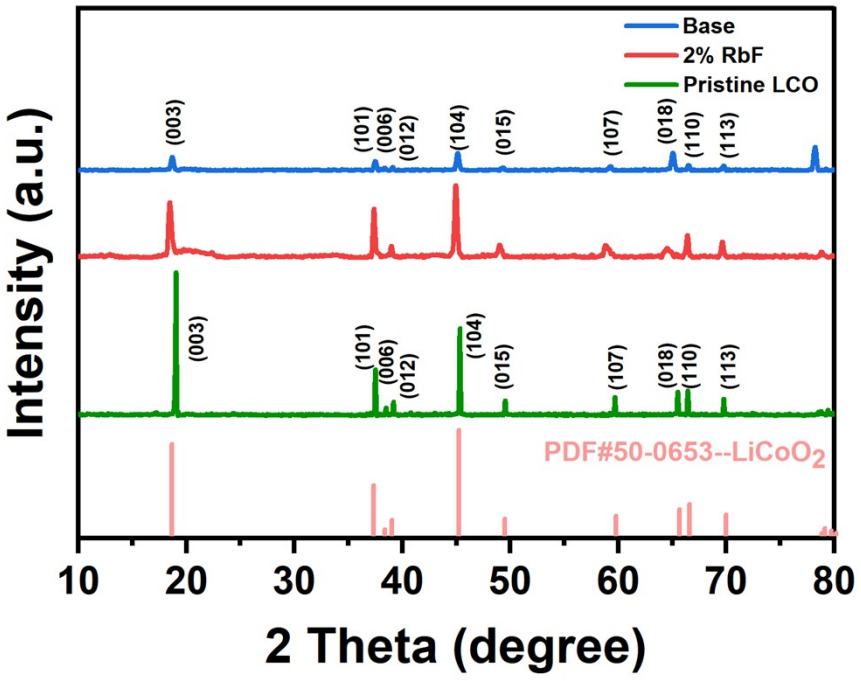

Figure S6. XRD of LCO cathodes after 200 cycles in pristine LCO, baseline and 2% RbF electrolytes.

Figure S7. The equivalent circuit diagram of fitted impedance values of Li||LCO batteries.

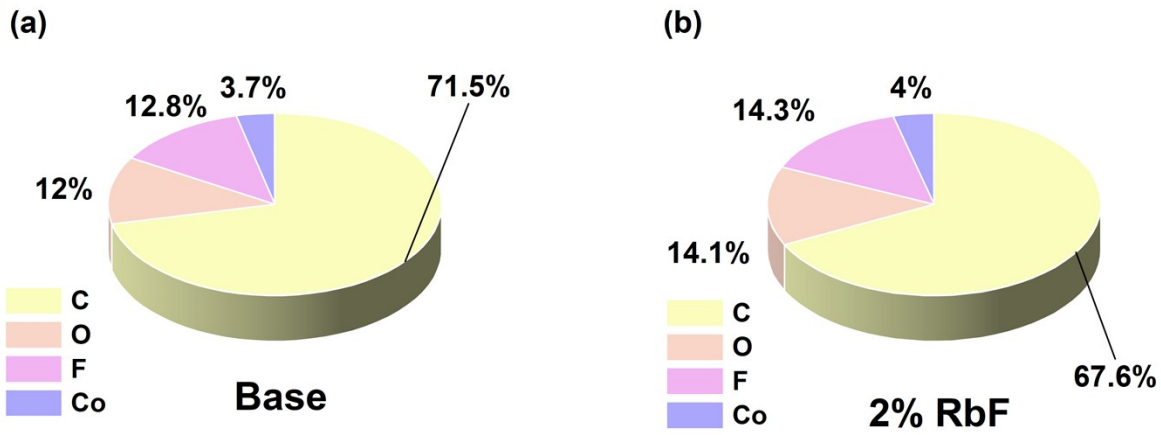

Figure S8. The atomic ratios of each major element were detected by element mapping of SEM in base (a) and 2% RbF (b) electrolytes.

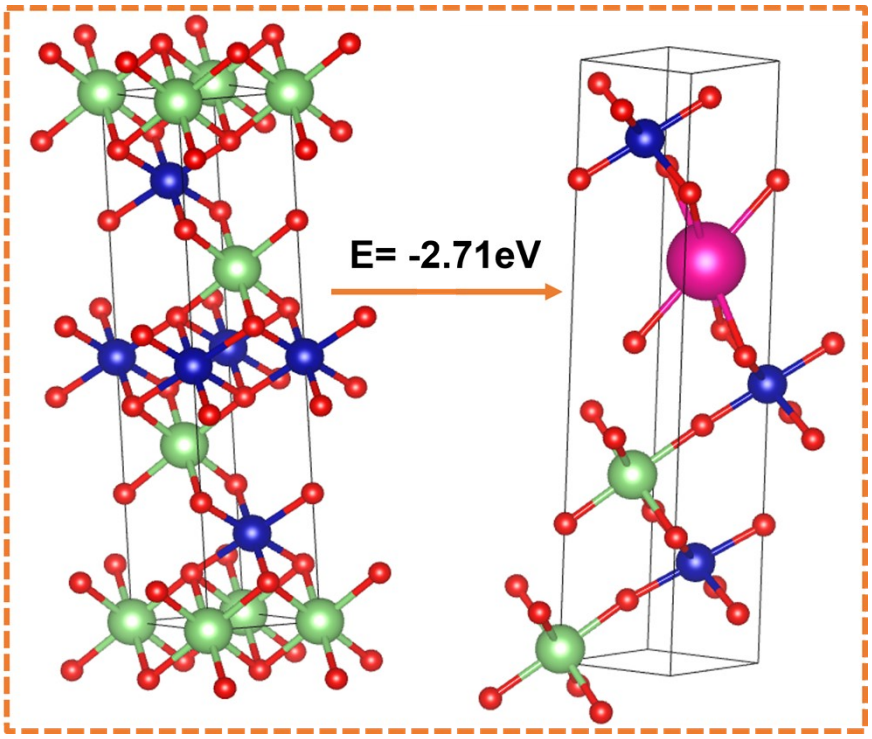

Figure S9. The adsorption energy of Rb^+ occupying the Li^+ vacancy in $LiCoO_2$.

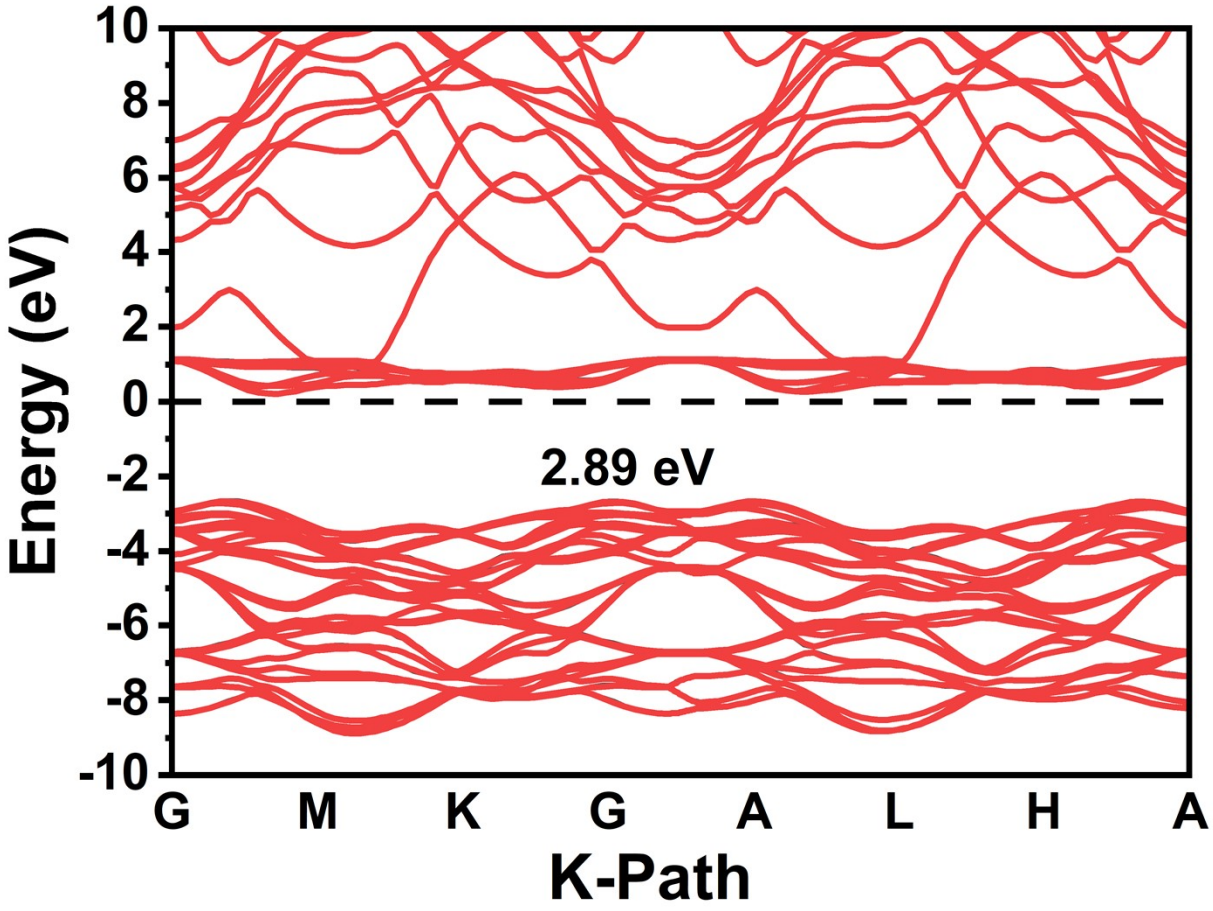

Figure S10. The band gap of LCO in 2% RbF electrolyte.

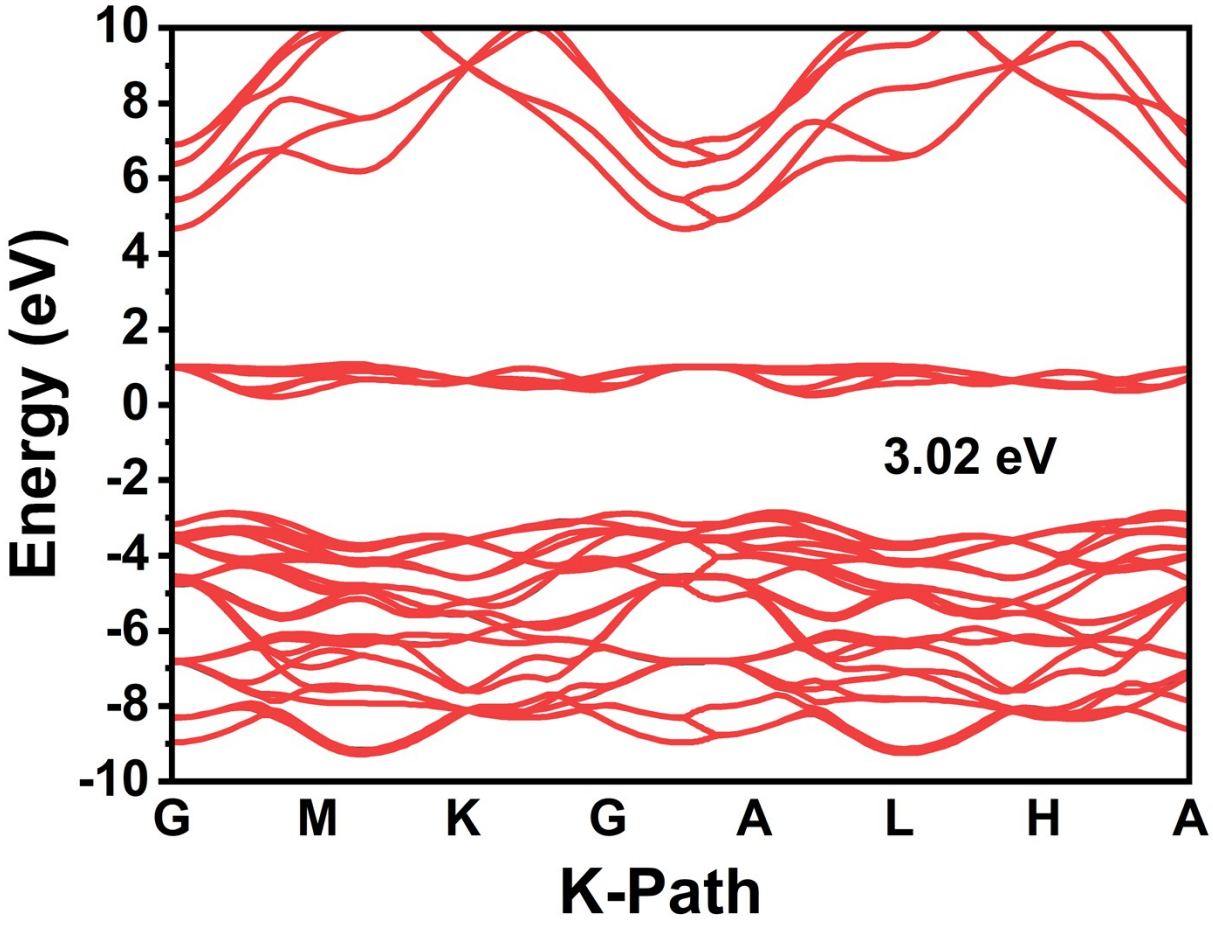

Figure S11. The band gap of LCO in based electrolyte.

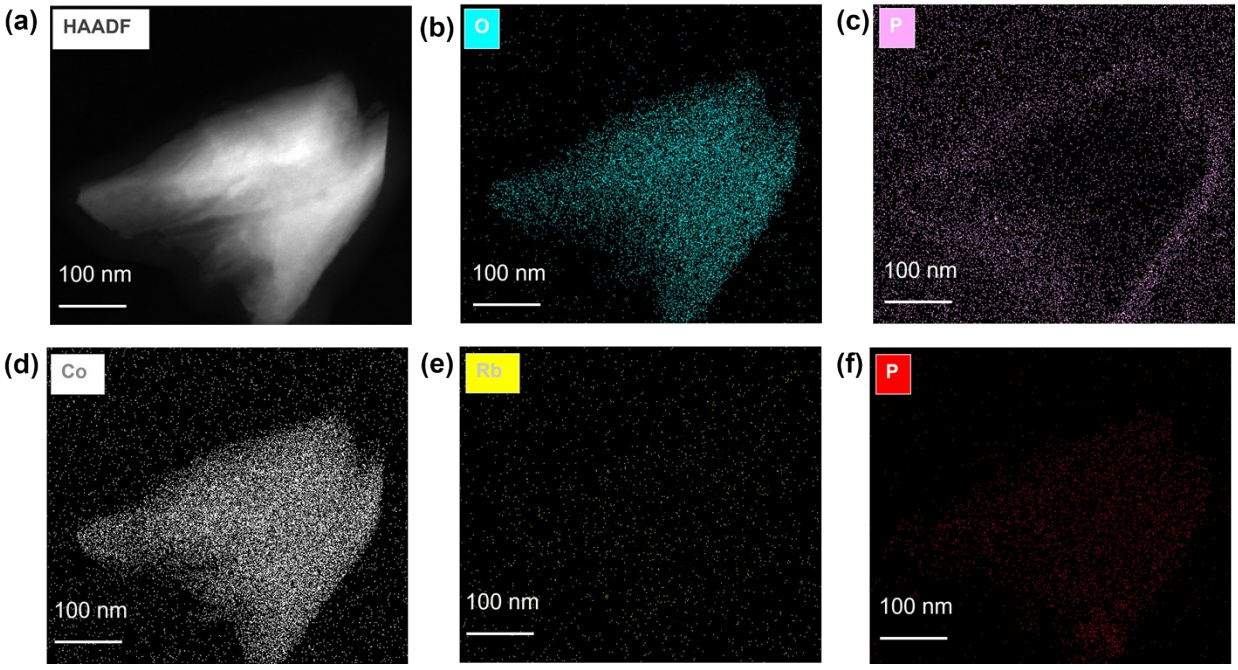

Figure S12. EDS mapping of LCO particle in RbF electrolyte.

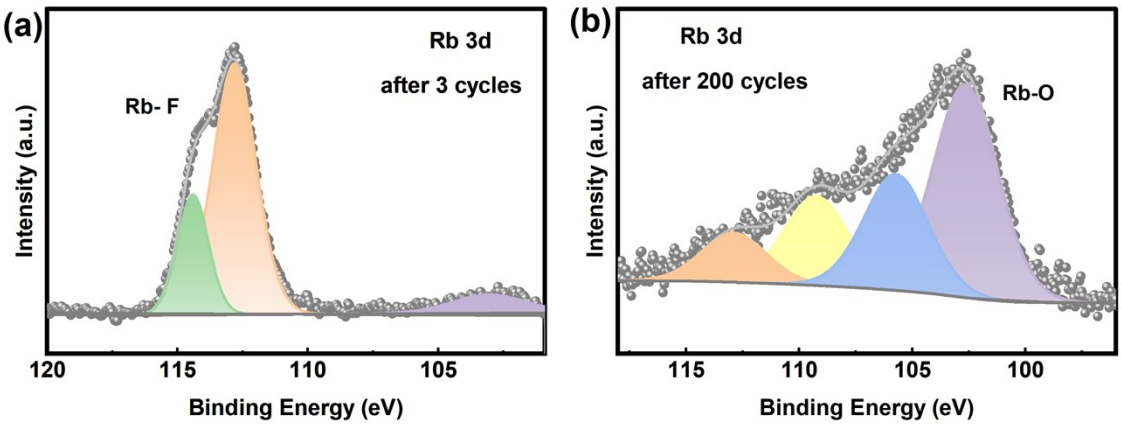

Figure S13. The Rb3d spectra of XPS on LCO cathodes after 3 and 200 cycles in 2% RbF electrolytes.

However, there are few XPS studies on Rb element, and the specific material composition cannot be completely determined temporarily, which is also the direction of future research.

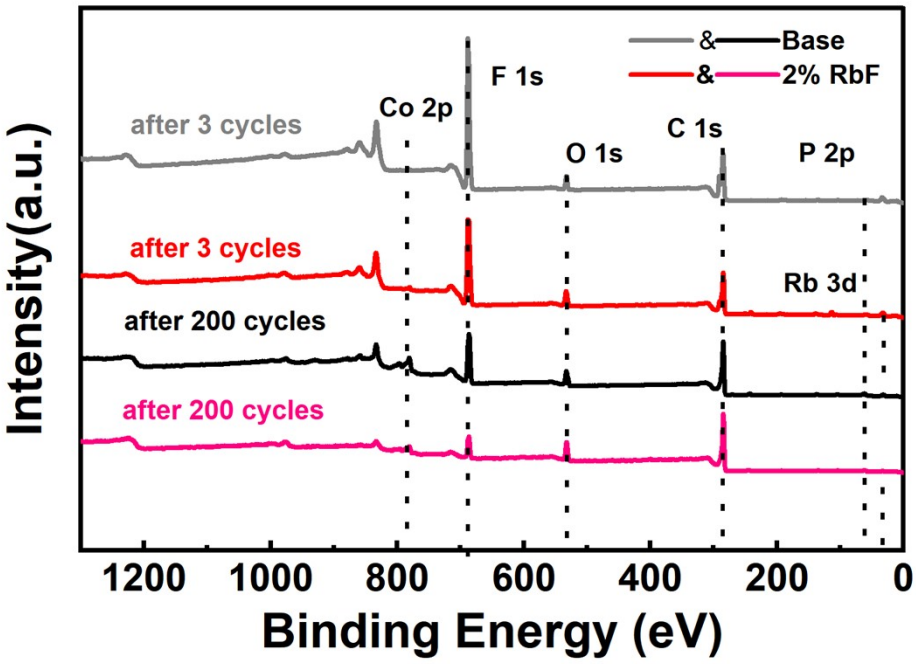

Figure S14. The survey XPS spectra of LCO cathodes after 3 and 200 cycles in baseline and 2% RbF electrolytes.

	Conductivity/ mS cm^{-1}	Viscosity/ cP
2% RbF	9.74	4.89
Base	8.65	3.90

Table S1. The conductivity and viscosity of two electrolytes.

Table S2. Comparison of electrochemical properties of reported LCO‖Li half cells with different methods to stabilize the high voltage LCO.

Method	Cell	Cut-off	Current Density / C	Capacity	Ref.

	configuration	Voltage / V	(1 C = 274 mA g^{-1})	Retention / %	
Electrolyte with 2 wt % RbF	LCO||Li	4.6	0.5	90 (200^{th})	This work
0.5% OIN-LCO	LCO||Li	4.6	0.5	82.5 (100^{th})	6
Sulfonamide-based electrolyte	LCO||Li	4.6	0.5	85 (100^{th})	7
TBAClO4/FEC-baseline electrolytes	LCO||Li	4.6	0.5	81 (300^{th})	8
FHP electrolyte	LCO||Li	4.6	1	76.1 (200^{th})	9
DPD-electrolyte	LCO||Li	4.6	1	69.2 (200^{th})	10
Electrolyte with 0.2 wt % KSeCN	LCO||Li	4.6	0.33 C (charge) 1 C (discharge)	81.8 (100^{th})	11
PL-LCO	LCO||Li	4.6	140 mA g^{-1} (0.5 C)	89.4 (200^{th})	12

References

1. G. Kresse and J. Furthmüller, *Physical review. B, Condensed matter*, 1996, **54**, 11169-11186.

2. P. E. Blöchl, *Physical Review B*, 1994, **50**, 17953-17979.

3. W. Hu, Y. Chen, H. kou, Y. Wang, H. Wan and H. Li, *Ionics*, 2022, **28**, 3139-3143.

4. Y. Chen, W. Hu, Q. Zhou and H. Li, *Journal of Solid State Electrochemistry*, 2021, **25**, 2565-2569.

5. M. H. Liu and C. W. Liu, *Journal of Molecular Modeling*, 2016, **23**, 4.

6. S. Mao, Z. Shen, W. Zhang, Q. Wu, Z. Wang and Y. Lu, *Advanced Science*, 2022, **9**.

7. W. Xue, R. Gao, Z. Shi, X. Xiao, W. Zhang, Y. Zhang, Y. G. Zhu, I. Waluyo, Y. Li, M. R. Hill, Z. Zhu, S. Li, O. Kuznetsov, Y. Zhang, W.-K. Lee, A. Hunt, A. Harutyunyan, Y. Shao-Horn, J. A. Johnson and J. Li, *Energy & Environmental Science*, 2021, **14**, 6030-6040.

8. W. Li, H. Wang, J. Zhang, H. Zhang, M. Chen, J. Wang, Y. Gao, R. Zhao, J. Hu, G. Feng, D. Zhai and F. Kang, *Advanced Energy Materials*, 2024, **14**.

9. C. Yang, X. Liao, X. Zhou, C. Sun, R. Qu, J. Han, Y. Zhao, L. Wang, Y. You and J. Lu, *Advanced Materials*, 2023, **35**.

10. Z. Sun, F. Li, J. Ding, Z. Lin, M. Xu, M. Zhu and J. Liu, *Acs Energy Letters*, 2023, **8**, 2478-2487.

11. A. Fu, J. Lin, Z. Zhang, C. Xu, Y. Zou, C. Liu, P. Yan, D.-Y. Wu, Y. Yang and J. Zheng, *ACS Energy Letters*, 2022, **7**, 1364-1373.

12. F. Zhang, N. Qin, Y. Li, H. Guo, Q. Gan, C. Zeng, Z. Li, Z. Wang, R. Wang, G. Liu, S. Gu, H. Huang, Z. Yang, J. Wang, Y. Deng and Z. Lu, *Energy & Environmental Science*, 2023, **16**, 4345-4355.